ASTRONOMY & ASTROPHYSICS
SUPPLEMENT SERIES

Astron. Astrophys. Suppl. Ser. **103,** 45-56 (1994)

Far-infrared spectra of cosmic-type pure and mixed ices

M.H. Moore[1] and R.L. Hudson[2]

[1] Astrochemistry Branch, Laboratory for Extraterrestrial Physics, NASA/Goddard Space Flight Center, Greenbelt, MD 20771, U.S.A.
[2] Department of Chemistry, Eckerd College, St. Petersburg, FL 33733, U.S.A.

Received *March 9*; accepted *June 1, 1993*

Abstract. — We have measured the far-infrared spectra of pure H_2O, CH_3OH, NH_3, CO_2, H_2CO, CH_4, and CO ices and H_2O-dominated binary mixtures of CH_3OH, NH_3, CO_2, H_2CO, CH_4, and CO from 500 cm^{-1} (20 μm) to 100 cm^{-1} (100 μm) at low temperatures. We also examined spectra of several more complex ices. These results represent a consistent set of data on astrophysically relevant molecules and mixtures over a wide range of temperatures. This set provides information in a spectral region that will be increasingly accessible with the advent of future orbiting observatories. Spectra of both the amorphous and crystalline phases of each of the pure molecular ices are unique. Spectra of icy mixtures, however, are in general dominated by H_2O ice features over the entire range of temperatures studied. One exception to this is the $H_2O + CH_3OH$ ice which evolves from an amorphous deposit to form a multi-line crystalline-like spectrum we have identified with the recently reported CH_3OH clathrate hydrate. Implications of these results on the identification of extraterrestrial ices based on observations in the far-infrared are included.

Key words: infrared: interstellar: lines — interstellar medium: clouds — molecular data — dust

1. Introduction

H_2O ice and H_2O-dominated icy mixtures are believed to be important constituents of interstellar grains, of comets, and of many of the outer planetary satellites. Extraterrestrial H_2O, CH_3OH, NH_3, CO_2, CO, and CH_4 in the condensed phase have all been identified by comparing observations made in the near-infrared or mid-infrared (extending typically from 10,000 cm^{-1} (1 μm) to 400 cm^{-1} (25 μm)) with laboratory reference spectra. These spectral regions include specific information on the stretching and bending modes of molecules. Examples of detections of condensed phase molecules are: H_2O, CH_3OH, NH_3, and CO_2 in dense interstellar clouds (Tielens 1989 and references therein; Allamandola et al. 1993; Graham & Chen 1991; and d'Hendecourt & de Muizon 1989, respectively), CO_2 and CO tentatively identified on Triton (Cruikshank et al. 1991), and CO and CH_4 on Pluto (Owen 1992).

Of all the extraterrestrial environments for ices, cold interstellar regions represent a promising place to search for far infrared (far-IR) signatures with relatively minimal conflicting background emissions. However, observations are limited because telescopes must operate from aircraft above the Earth's lower atmosphere which is opaque between 250 cm^{-1} (40 μm) and 33 cm^{-1} (300 μm). An example of an early far-IR observation of a dense interstellar cloud region, is the detection of the 222 cm^{-1} (45 μm) feature in Orion's Kleinman-Low nebula (Papoular et al. 1978; Erickson et al. 1981, and Drapatz et al. 1983) which was interpreted as due to H_2O ice. Later, Forveille et al. (1987) observed a striking increase in the 167 cm^{-1} (60 μm) band of IRAS 09371 and proposed that H_2O ice emission was responsible; a large quantity of ice was confirmed by the mid-IR detection of H_2O ice (Rouan et al. 1988; Hodapp et al. 1988 and Geballe et al. 1988). The recent more detailed observations of IRAS 09371 by Omont et al. (1990) showed an emission band in the 250 cm^{-1} (40 μm) to 143 cm^{-1}(70 μm) region which they fitted with the spectrum of crystalline H_2O ice on crystalline silicate grains at 46 K. Omont et al. (1990) also published data for OH 127.8 and OH 231.8 in the far-IR.

H_2O and other simple polyatomic molecules condense to form molecular crystals which have, compared to near-IR and mid-IR spectra, broad far-IR features due to lattice modes (intermolecular vibrations). These modes involve the relative motion of the molecules as a whole and can be either translational modes (displacements) or librational modes (torsional in origin). The far-IR intramolecular modes often give information on lattice structure or transitions between phases. Amorphous H_2O ice, for

Send offprint requests to: M.H. Moore, NASA/Goddard Space Flight Center, Code 691, Greenbelt, Maryland 20771

example, formed by condensation at $T < 100$ K, is not stable against thermal cycling. It converts irreversibly to a polycrystalline phase during warming to $T > 120$ K. The far-IR spectra of H_2O show distinct differences between the amorphous and crystalline phases.

Our previous far-IR laboratory investigations focused on the phase changes in H_2O ice induced by proton irradiation and were motivated by the identification of crystalline H_2O at 46 K by Omont et al. (1990) in IRAS 09371. Our studies resulted in estimates of the rate of radiation amorphization of crystalline ice in simulated cosmic environments (see Moore & Hudson 1992 and references therein). In those experiments we also examined the thermally induced phase change of H_2O and the reversible changes in the peak position of the principal maximum at 222 cm^{-1} (45 μm) with temperature.

In the present work we have measured the far-IR spectra of pure amorphous and annealed crystalline CH_3OH, NH_3, CO_2, and H_2CO ices. These pure ices have absorption peaks which, like H_2O, show reversible and irreversible changes with temperature. This data set also includes the far-IR spectra of H_2O -dominated binary mixtures of these same molecules, along with CH_4 and CO, in the amorphous and annealed crystalline phases. The most unique far-IR spectrum resulted when an $H_2O + CH_3OH$ (100:50) mixture was slowly warmed resulting in a characteristic set of absorption bands which we have identified (Hudson & Moore 1993) with the recently reported CH_3OH clathrate hydrate (Blake et al. 1991).

It is our intention that this set of data be a source of peak positions of some relevant molecular ices in different phases in the far-IR. This set is unique because it represents the use of a single experimental procedure to study a large number of pure and mixed ices of interest to astronomers over a variety of temperatures which are astrophysically relevant.

2. Experimental procedure

Figure 1 is a schematic representation of the experimental setup. Thin icy films were formed by slowly condensing either pure or premixed gases onto an aluminium substrate (5 cm^2 area) cooled by a closed-cycle cryostat ($T_{min} \sim 13$ K). Surrounding the substrate is a six-sided vacuum chamber designed to allow a variety of in-situ measurements. The ice film is shown facing the IR spectrometer, but it could also be rotated to face any direction. Far-infrared absorption spectra were recorded with a Mattson (Polaris) Fourier-transform infrared (FTIR) single-beam spectrometer equipped with a 6 μm mylar beam splitter. Using a focus projection attachment, the IR beam was directed at right angles to the spectrometer bench, through a 1.6 mm thick high-density polyethylene window, where it passed through the ice film, reflected at the ice-aluminum interface, and again passed through the ice film before traveling to the detector. We used this technique to measure the transmission-reflection-transmission spectra (TRT-spectra) from 500 cm^{-1} to 100 cm^{-1} (20 μm to 100 μm) as 60-scan accumulations ($\sim$ 3 min total accumulation time) with a resolution of 4 cm^{-1}. It has been recognized that band intensities and widths may differ slightly between transmission spectra and TRT-spectra, although the line positions should be the same (e.g. Kitta & Kträtschmer 1983). In general our far-IR TRT data for H_2O and NH_3 (the ices with the highest reflectivities) had a slightly larger area when normalized to a spectrum recorded in transmission. We attribute this to the fact that we detect the attenuated beam component along with some fraction of the reflected beam (see Hudson & Moore 1993). Spectra presented in this paper have not been corrected for reflection losses.

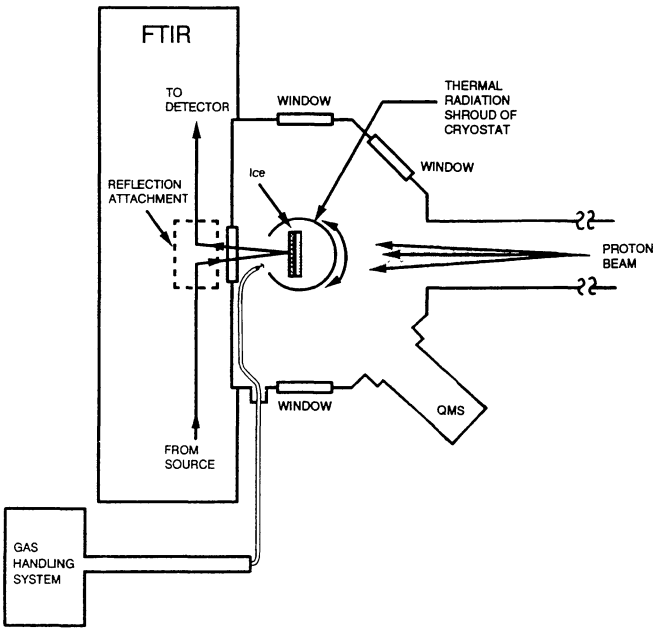

Fig. 1. Experimental set-up showing the FTIR, QMS (quadrupole mass spectrometer), incoming proton beam, and central location of the cryostat containing the ice films

Each single-beam spectrum was ratioed with the background spectrum of a blank substrate at 13 K. Absorptions due to any residual water vapor within the optical path had minimal effect on the ratioed spectra if the background and single beam spectra were recorded with the same dry nitrogen purge conditions. Apparent noise in some spectra is due to incomplete cancellation from varying purge conditions.

The water used to make the ice samples was triply distilled with a resistance greater than 10^7 ohm-cm and with dissolved gases removed by freeze-pump-thaw cycling. Methanol (American Burdick and Jackson, HPLC grade) was also degassed by freeze-pump-thaw cycling.

Ammonia (Matheson, anhydrous), carbon dioxide (Air Products, 99.5% pure), methane (Matheson, UHP grade) and carbon monoxide (Airco, 99.99% pure) gases were used without further purification. solid paraformaldehyde (Fisher Scientific Co., purified) was warmed in a vacuum bottle to produce monomeric formaldehyde.

Thin films of amorphous ices were in general less than 10 μm thick (determined by using appropriate optical constants) and were condensed at a rate of $\sim$ 10 μm hr^{-1}. Amorphous H_2O, CH_3OH, NH_3, CO_2, and H_2CO were warmed from 13 K to 155 K, 130 K, $\sim$ 110 K, 65 K and 85 K respectively, and held there about 5 minutes to convert them to a crystalline phase. The ice samples could be rotated 180° from the direction of the FTIR to face the proton source which was permanently interfaced with our experimental set-up. Details of the proton source and techniques for monitoring the resulting dose (protons cm^{-2}) have been discussed elsewhere (Moore & Hudson 1992).

3. Experimental results

Far-IR spectra of pure, binary, and several more complex ices have been measured from 500 cm^{-1} to 100 cm^{-1} (20 μm to 100 μm) at temperatures from 13 K to 165 K. Spectra of pure H_2O taken from earlier publications (Moore & Hudson 1992), are included for completeness. The absorbance scale in our figures has been expanded arbitrarily unless otherwise specified.

3.1. *Far-IR spectra of amorphous and crystalline pure ices*

The far-IR spectra of H_2O, CH_3OH, NH_3, CO_2, H_2CO, CH_4, and CO have been measured from 500 cm^{-1} to 100 cm^{-1} over a temperature range from 13 K to as high as 155 K. Figures 2 and 3 compare the spectra of these ices in the amorphous and crystalline phases, respectively. Spectra have been offset for clarity. All curves have the absorbance scale shown for Fig. 2g. Some spectra are displayed at different magnifications (as indicated). Table 1 lists the corresponding peak positions.

3.1.1. H_2O

The far-IR bands of amorphous and crystalline H_2O ice at 13 K are shown in Fig. 2a and Fig. 3a respectively. When the amorphous ice (peak position, 220 cm^{-1}, 45.5 μm) was warmed, its spectrum changed irreversibly into the sharper crystalline form with absorptions at 223 cm^{-1} (44.8 μm) and 158 cm^{-1} (63.3 μm). Noticeable sublimation of H_2O ice occurs within 5 to 10 minutes at a temperature of 170 K. The ice's physical thickness is estimated to be $\sim$ 2.5 μm based on absorption coefficients at 10 K for amorphous H_2O (Hudgins et al. 1993). Documentation of changes in the amorphous and crystalline

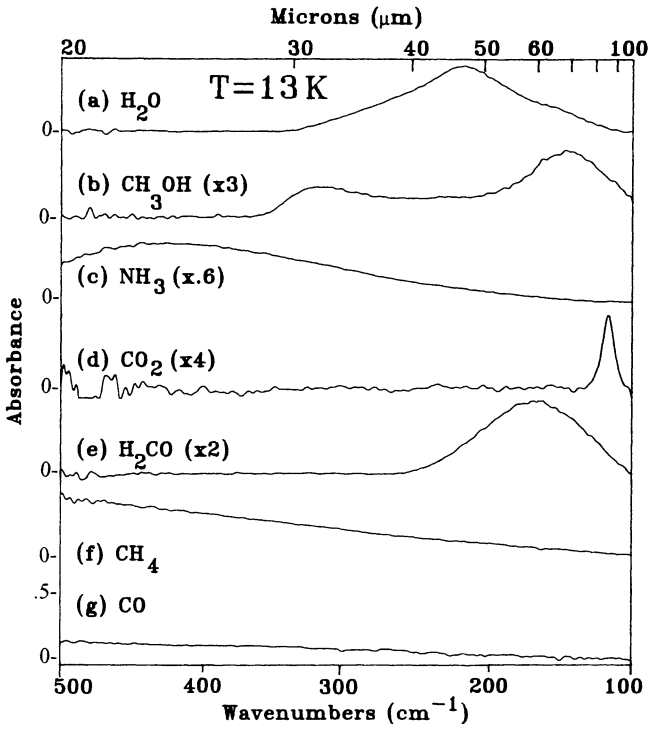

Fig. 2a-g. Far-IR spectra of pure amorphous ices deposited at $T \sim 13$ K; peak positions are listed in Table 1

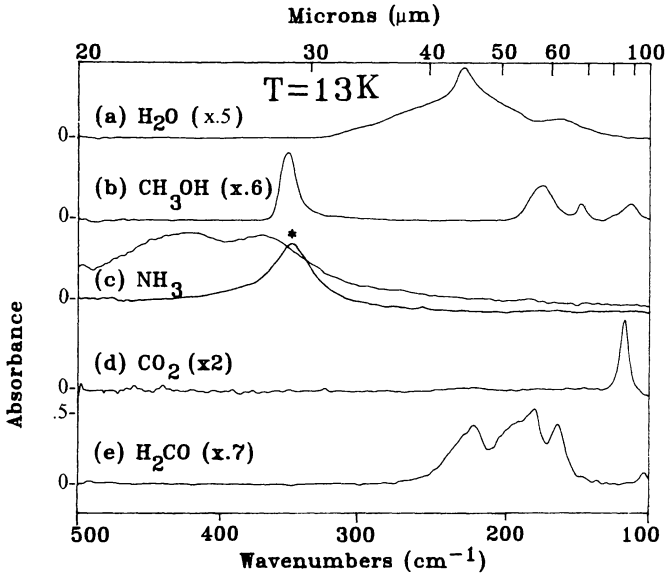

Fig. 3. Far-IR spectra of pure crystalline phase ices of (a) H_2O, (b) CH_3OH, (c) NH_3 (double peaked), (d) CO_2 and (e) H_2CO were formed by annealing at 155 K, 130 K, $\sim$ 110 K, 65 K and 85 K respectively; peak positions are listed in Table 1 (the single * NH_3 peak results after direct deposit at 77 K before recooling to 13K)

far-IR spectra as a function of temperature has been discussed in an earlier publication (Moore & Hudson 1992)

and has also been examined by Breukers (1991). Some of these results are included in this paper for comparison with other molecular ices.

3.1.2. CH_3OH

The far-IR bands of amorphous and crystalline CH_3OH are shown in Fig. 2b and Fig. 3b respectively. The ice sample's physical thickness is estimated to be ~ 3.5 μm based on the absorption coefficient at 10 K for amorphous CH_3OH (Hudgins et al. 1993). The change from amorphous (peak positions 321 and 148 cm^{-1}) to crystalline (peak positions, 353, 175, 147, 113 cm^{-1}) begins between 100 K and 120 K and is completed in 5 minutes by raising the temperature to 130 K. Noticeable sublimation of the sample occurs within 5 to 10 minutes at a temperature of 155 K.

3.1.3. NH_3

The far-IR bands of NH_3 in the amorphous, and crystalline phases are shown in Fig. 2c and Fig. 3c respectively. The ice's physical thickness is estimated to be ~ 0.5 μm based on the absorption coefficient for cubic crystalline NH_3 at 88 K (Sill et al. 1980). When amorphous deposits (peak at 423 cm^{-1}) were warmed slowly, a double-peaked (422 cm^{-1} and 372 cm^{-1}) spectrum was observed to form between 60 K and 70 K. We call this a transition phase. The double-peaked spectrum evolved with increased warming (several hours at 105 K, or by pulsing the ice temperature to 120 K) into an asymmetrically shaped single peaked spectrum (resulting peak position is 352 cm^{-1} after recooling to 13 K). Some subblimation of the sample occurred at these higher annealing temperatures. A symmetrically shaped, single-peaked spectrum of NH_3 ice, attributed to cubic phase NH_3, was formed by directly condensing NH_3 at 77 K in agreement with Sill et al. (1980).

3.1.4. CO_2

The far-IR bands of amorphous and crystalline CO_2 are shown in Fig. 2d and Fig. 3d respectively. The ice's physical thickness is estimated to be ~ 2.5 μm based on the absorption coefficient at 100 K (Warren, 1986). When the amorphous ice (single peak at 117 cm^{-1}) is slowly warmed it converts to a sharper crystalline peak between 60 K to 65 K. Changes in the line width and intensity are not obvious when comparing Fig. 2d and Fig. 3d because of the scaling factor used in Fig. 2d. Sublimation is observed when the ice is maintained at $T > 100$ K.

3.1.5. H_2CO

The far-IR bands of amorphous and crystalline H_2CO are shown in Fig. 2e and Fig. 3e respectively. The ice thickness is estimated to be on the order of a few micrometers based on the amount of gas deposited. The thickness was not calculated more precisely because absorption coefficients are not known. When the amorphous ice (single peak at 164 cm^{-1}) was slowly warmed it converted to the crystalline phase above $T = 70$ K (peak positions at $T = 13$ K are: 223, 191 shoulder, 180, 164, and 103 cm^{-1}). Rapid sublimation was observed beginning at 110 K.

3.1.6. CH_4 and CO

CH_4 and CO have absorptions at frequencies lower than our 100 cm^{-1} cut-off (Savoie & Fournier 1970; Ron & Schnepp 1967, respectively). Deposits of each ice resulted in a relatively straight line showing greater absorbance at higher frequencies (Figs. 2f and 2g). Rapid sublimation of both CH_4 and CO was detected between 45 K and 55 K using a mass spectrometer.

3.2. *Temperature dependence of peak frequencies of several crystalline ices*

The peak frequency of the principal maximum of crystalline H_2O changed reversibly with temperature (Breukers 1991; Moore & Hudson 1992). Figure 4 shows data for H_2O compared with the following: the most intense absorption of solid CH_3OH near 353 cm^{-1}, NH_3 near 352 cm^{-1}, H_2CO near 223 cm^{-1} (chosen because this band remains unobscured over the temperature range), and CO_2 near 117 cm^{-1}. Included for completeness are data from other experimenters for similarly prepared ices. The solid lines are least squares fits of our measured data points; usually the lower temperature data points were not included in the fits because the peaks typically do not change much below 30 K to 40 K. The peak frequency of each ice shifts to lower frequencies as the temperature increases and can be directly related to the ice's temperature.

3.3. *Far-IR spectra of amorphous and crystalline binary icy mixtures*

The spectra of amorphous and crystalline H_2O-dominated icy mixtures containing $\sim 12\%$ of an added molecule are shown in Fig. 5. Spectral pairs are offset for clarity. Peak positions are tabulated in Table 2. Pure H_2O is included in Fig. 5a for reference. The amorphous binary ice deposits reflect the broad symmetrical band shape of pure amorphous H_2O, although, there is a trend for the maximum to occur at a slightly lower frequency in the mixtures. Mixtures were annealed to 155 K for 5 minutes to induce crystallization, and then recooled to 13 K. Spectra of the crystalline mixtures are dominated by a sharp peak near 223 cm^{-1} (44.8 μm) like that of pure H_2O. Many had a secondary peak similar in position to the one seen in pure H_2O ice. Spectra compared after normalizing at the principal maximum, show that the ratio between the peak absorbances of the principal and secondary maximum was always smaller in the mixtures.

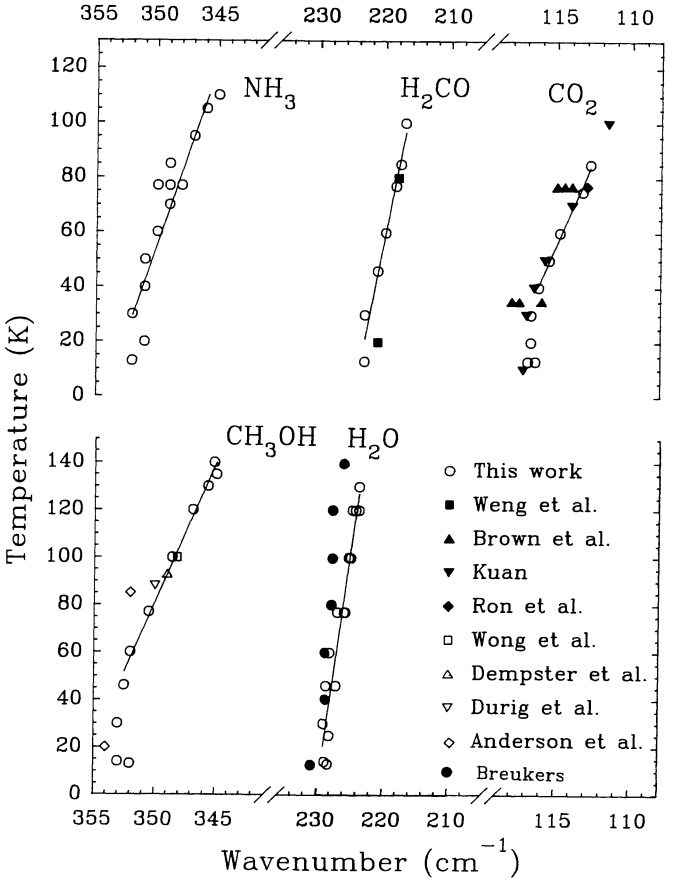

Fig. 4. Reversible changes in peak frequencies for crystalline ices as a function of temperatures: NH_3 data for 352 cm^{-1} peak, H_2CO data for 223 cm^{-1} peak, CO_2 data for 117 cm^{-1} peak, CH_3OH data for 353 cm^{-1} peak, and H_2O data for 230 cm^{-1} peak

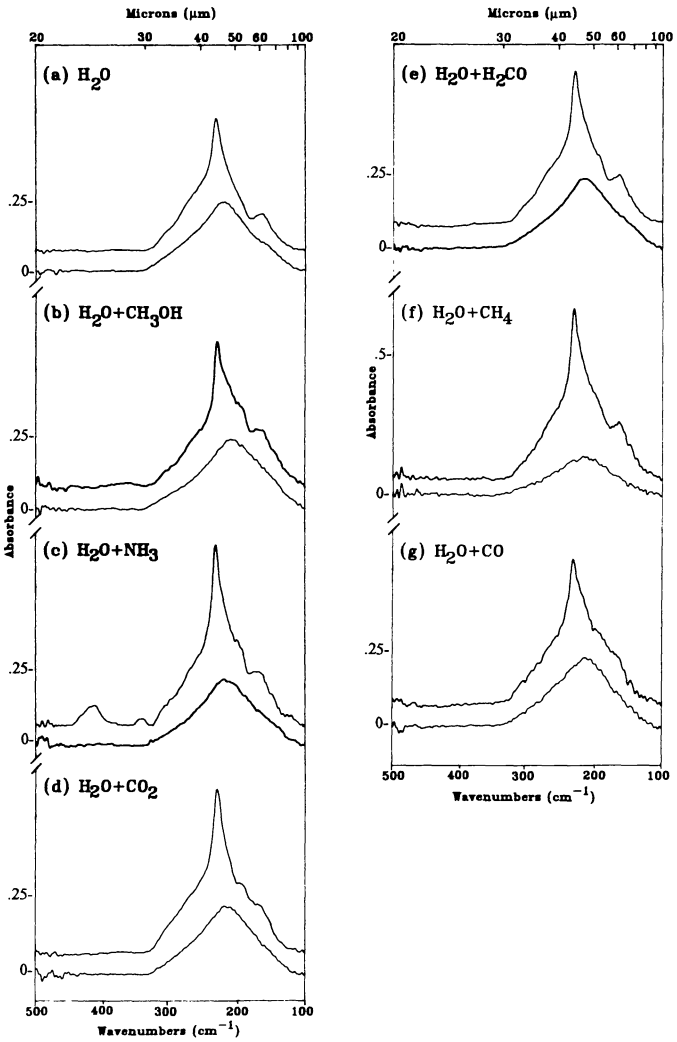

Fig. 5. (a) Far-IR spectra of pure amorphous and crystalline phase H_2O ice is compared with the far-IR spectra (b-g) of amorphous and crystalline phase ices of H_2O combined with CH_3OH, NH_3, CO_2, H_2CO, CH_4 and CO (~ 100:12)

The FWHM (full width at half maximum) of the mixtures varied within 20% of that of pure H_2O.

3.4. *Mixtures selected for concentration and temperature study*

The far-IR spectra of an H_2O+CO_2 mixture was examined at two different concentrations. When the concentration of CO_2 is ~ 12% (compared to H_2O) the amorphous spectrum is indistinguishable from that of amorphous water. With an equal amount of H_2O and CO_2, the amorphous spectrum has a high frequency broad absorption near 400 cm^{-1} along with the lower frequency feature. Figure 6 shows these spectra compared to the spectra of amorphous pure H_2O and CO_2. The 400 cm^{-1} absorption decreased with increasing temperatures and was gone at 120 K. Both of these mixtures resulted in an annealed spectrum whose primary maximum is located near 230 cm^{-1} (the boxed-in inserts in Fig. 6 show the annealed spectra).

Mixtures of $H_2O + CH_3OH$ were also selected for a concentration and temperature study. The results are summarized in Figs. 7 and 8. When the concentration of CH_3OH is ~ 12% (compared to H_2O) the amorphous spectrum shows one broad absorption feature resembling amorphous water with a high frequency tail. With an ~ 50% CH_3OH concentration, the broad absorption feature has a distinguishable CH_3OH shoulder in the 300 cm^{-1} region. The evolution of this mixture with increased temperature is followed in Fig. 8. Figure 8a is the amorphous deposit at 13 K. Warming this ice to 130 K < T < 140 K at a rate of 3-6 K min^{-1} resulted in the spectrum in Fig. 8b. Either holding the sample at this temperature for several hours or warming to 145 K < T < 148 K for less than 15 min, resulted in the simultaneous growth of the five absorption features shown in Figs. 8c, 8d, and 8e. These absorptions sharpened as the temperature was reduced, and one feature split into two components at 13 K (Fig. 8f). The identification of

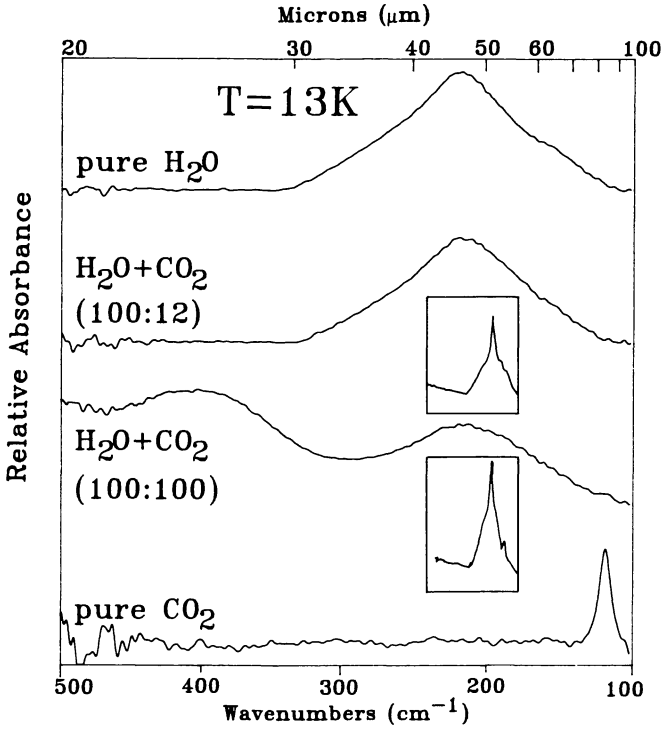

Fig. 6. Far-IR spectra of amorphous ices formed from two different concentrations of an $H_2O + CO_2$ mixture are compared with spectra of pure amorphous H_2O and CO_2 ices; spectra of both annealed mixtures are shown in the inserts

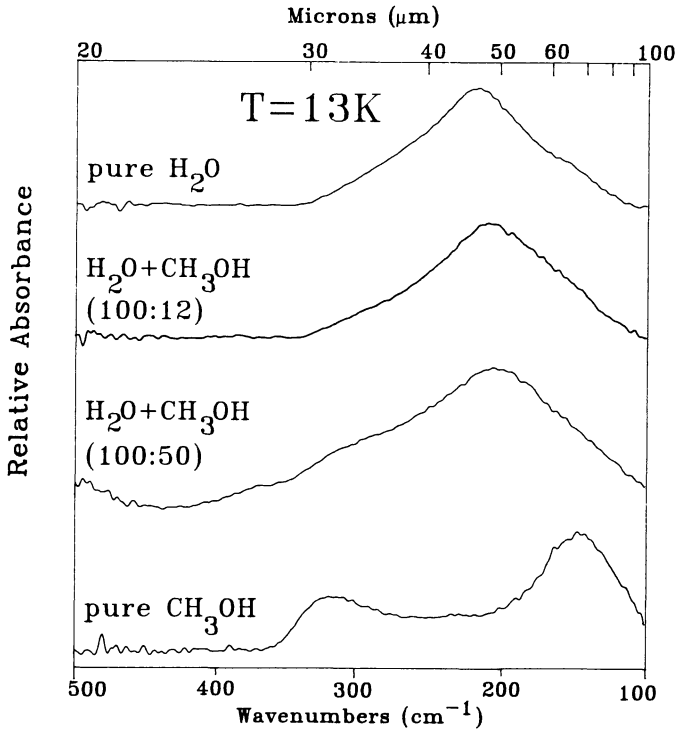

Fig. 7. Far-IR spectra of amorphous ices formed from two different concentrations of an $H_2O + CH_3OH$ mixture are compared with spectra of pure amorphous H_2O and CH_3OH ices

this far-infrared multi-line spectrum with the clathrate hydrate and a discussion of the x-ray diffraction studies which led to the original identification of the methanol clathrate hydrate using a similar formation method is given elsewhere (Hudson & Moore 1993 and Blake et al. 1991, respectively). The clathrate spectrum is quite different from that of either pure CH_3OH or pure H_2O as shown in the insert spectrum in Fig. 8. Table 3 includes the peak positions for the CH_3OH clathrate hydrate at 13 K and at 148 K.

3.5. *Far-IR spectra of multi-component ices*

We studied two ices made of a multi-component mixture (a more realistic simulation of proposed interstellar ices) with two different concentrations: $H_2O + CH_3OH + CO + NH_3$ (100:50:2:2 and 100:50:9:2). We wanted to examine what effect the addition of other molecular species had on the far-IR spectrum. Figure 9 compares the spectra of these two multi-component ices (formed by slow warming) with the spectrum of $H_2O + CH_3OH$ (100:50) warmed to $T > 145$ K. Spectra have been offset for clarity. Figure 9a is the methanol clathrate at 148 K (distinctive methanol clathrate peaks are marked with an asterisk). These peaks are somewhat weaker in the spectra at 155 K when 2% NH_3 and 2% CO relative to water were present in the mixture (Fig. 9b). The spectrum at 150 K shows that the characteristic multi-line features of the methanol clathrate are substantially weaker when 9% CO and 2% NH_3 relative to water were included. Peak frequencies for spectra shown in Fig. 9 are included in Table 3. Spectra of other multi-component mixtures formed by including CO, NH_3, CO_2, or H_2CO in an $H_2O + CH_3OH$ (100:50) mixture (spectra not shown) supported our observation that the characteristic multi-line features of the methanol clathrate are weakened when impurities are added.

3.6. *Far-IR spectra of proton irradiated methanol clathrate*

Figure 10 shows a sequence of far-IR spectra of the CH_3OH clathrate hydrate before (Fig. 10a), and after proton irradiation. Spectra are offset for clarity. The multi-line spectrum of the CH_3OH clathrate hydrate shown in Fig. 10a becomes less intense with increasing doses of radiation (Figs. 10b and 10c). After a dose of 10^{15} protons cm^{-2} (Fig. 10d), the spectrum is indistinguishable from the broad underlying absorption. The irradiated ice was warmed-up to see if the clathrate pattern would reappear, but only a single peaked spectrum similar to pure amorphous H_2O (Moore & Hudson, 1992, see Fig. 5) was formed. Continued warming of this ice converted it to a

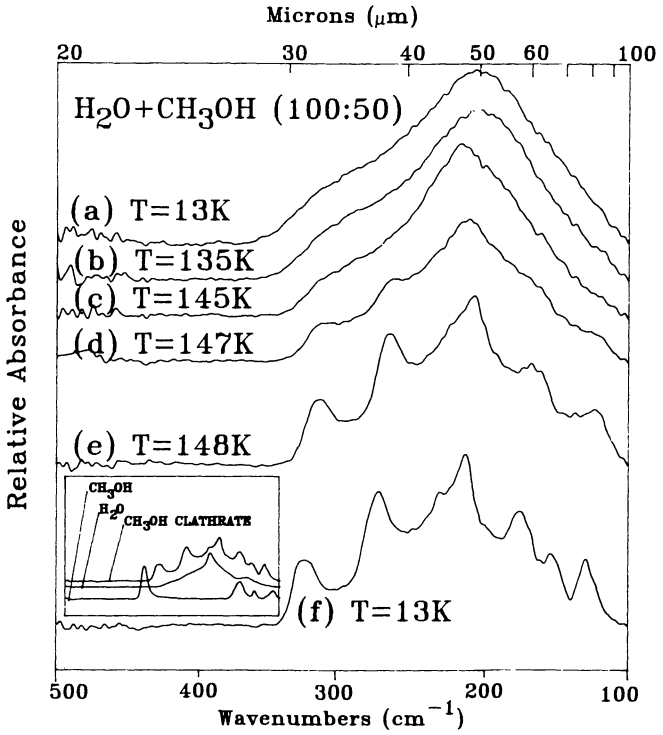

Fig. 8a-f. Evolution of the far-IR spectrum of an H_2O + CH_3OH mixture during warming shows the development of multi-line features associated with the CH_3OH clathrate hydrate; the insert spectra demonstrate there are many differences between the spectrum of the CH_3OH clathrate hydrate at 13 K and the spectrum of either pure crystalline CH_3OH or H_2O (peak positions listed in Table 3)

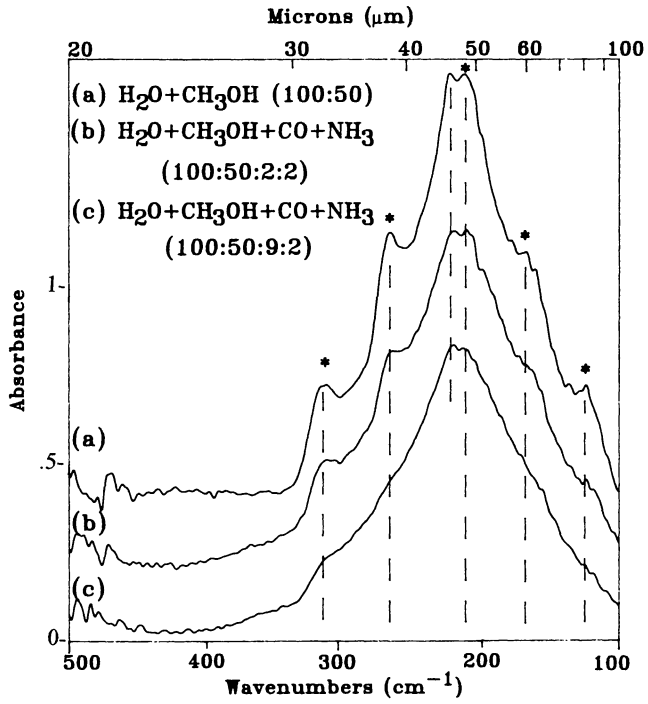

Fig. 9. (a) The multi-line far-IR features associated with the methanol clathrate at $T > 145$ K (marked with an *) are compared with the weaker "clathrate-like" features formed in more complex ices shown in b and c warmed to $T = 155$ K and $T = 150$ K respectively (peak positions listed in Table 3); peak near 222 cm^{-1} (45 μm) is attributed to crystalline H_2O

crystalline, H_2O-like spectrum which is shown in Fig. 10f (ice was recooled to 13 K).

4. Discussion

4.1. *Pure ices*

The far-IR spectra of pure H_2O and its conversion from the amorphous to the crystalline phase is discussed in detail in an earlier paper (Moore & Hudson 1992). A brief summary is included here since other spectra we discuss are compared with H_2O and the dominant species in our icy mixtures is H_2O. The low temperature ($T = 13$ K) amorphous form of H_2O has a single broad symmetrical band centered at 220 cm^{-1} (45.5 μm) (Moore et al. 1992; Hudgins et al 1993). This peak sharpens and shifts to lower frequencies as the temperature is raised. The irreversible conversion of amorphous H_2O to the crystalline form is complete at 155 K in about 10 minutes. The absorptions at 223 cm^{-1} (44.8 μm) and at 162 cm^{-1} (61.7 μm) in the crystalline phase correspond to the transverse optical and longitudinal acoustic vibrational modes. The libration mode of H_2O lies beyond our 500 cm^{-1} (20 μm) high frequency cut-off. Optical constants in the far-IR for H_2O ice are discussed by Bertie et al. (1969) and Hudgins et al. (1993).

Our spectra show that the amorphous form of CH_3OH has two broad bands centered at 319 cm^{-1} (31.3 μm) and 148 cm^{-1} (67.6 μm) at 13 K. These bands are in good agreement with the spectra and optical constants recently published by Hudgins et al. (1993). After warming amorphous CH_3OH to 130 K a stable spectrum with sharper and more numerous peaks was formed which we identify with the crystalline α-phase of CH_3OH in agreement with Wong & Whalley (1971). At $T = 13$ K, lattice vibrations were measured at 353, 175, 147 and 113 cm^{-1} (28.3, 57.1, 68.0, and 88.5 μm respectively). A higher temperature β-phase, stable between 160 K and 170 K was not examined. The 353 cm^{-1} and 147 cm^{-1} peaks are in close agreement with the positions published by Anderson et al. (1988) at 20 K; they associated these with the translational and librational modes respectively. We do not see the weaker features reported by Anderson et al. (1988) at 328, 278, 231, and 216 cm^{-1}, and our lowest frequency band is at 113 cm^{-1} not at 121 cm^{-1}. The position of our strongest bands at 100 K (spectra not shown in this paper) agree with published spectra recorded in the 80 K to 100 K range by Dempster & Zerbi (1971), Durig et al. (1971), Wong & Whalley, (1971) and Anderson et al. (1988).

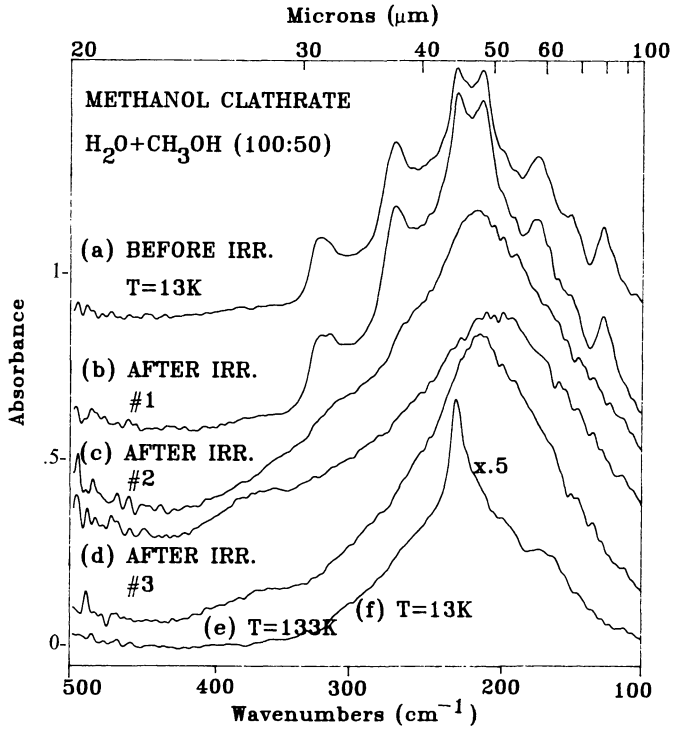

Fig. 10. (a) The far-IR spectrum at 13 K of a methanol clathrate before irradiation, (b-d) increasing amounts of radiation (#1, #2, #3 doses represent 10^{13}, 10^{14}, 10^{15} protons cm^{-2}, respectively) weaken the multi-line clathrate pattern, (e) rewarming the irradiated ice does not reform the clathrate structure, (f) far-IR spectrum at 13 K after annealing the irradiated ice to 155 K results in crystalline H_2O-like features (peak positions listed in Table 3)

The low temperature amorphous form of NH_3 has one broad band centered at 423 cm^{-1} (23.6 μm). During warming from 60 K to 70 K the spectrum changed to two overlapping peaks of similar intensity near 422 cm^{-1} and 372 cm^{-1} (23.7 μm and 26.9 μm). This double-peaked transition phase, probably associated with the metastable phase of NH_3, evolved with warming as the higher frequency component decreased. Annealing these metastable ices to 115 K to convert them to the cubic crystalline phase was, however, not entirely successful because of the rapid sublimation of NH_3. At 115 K the loss rate for the thin films was greater than the conversion rate to the cubic phase. Nevertheless, the dominant peak in our NH_3 ices (annealed to 115 K and recooled to 70 K) is 355 cm^{-1} (28.2 μm); these ices retained a short wavelength shoulder and are most likely part cubic and part metastable. Ices deposited at 77 K show a symmetrical peak. This absorption band is attributed to a librational mode (see e.g. Ferraro et al. 1980). The position of the most intense peak at 355 cm^{-1} is different from the published value of 360 cm^{-1} (27.8 μm) for cubic NH_3 deposited at 83 K $< T <$ 100 K and recorded on a variety of substrates (see Ferraro et al. 1980; Sill et al. 1980; Binbrek & Anderson 1972; Redding & Hornig 1951; Anderson & Gebbie 1965; Anderson & Walmsley 1965). The difference in the position of the maxima between our experiments and others may be due to one or more of the following: (1) internal reflections which have not been corrected in our experiments which may cause a peak frequency dependance on thickness, (2) reflected radiation reaching the detector (a consequence of the configuration when measuring TRT-spectra) which could be significant since NH_3 has a reflectivity near 65% at 355 cm^{-1} (Martonchik et al. 1984) (this reflectivity is larger than the reflectivity calculated for any other ice we studied in the far-IR). Our transition phase and cubic phase NH_3 spectra also showed weaker absorptions which agree with published values at 258 cm^{-1} (38.8 μm), attributed to another libration mode, and at 183 cm^{-1} and 138 cm^{-1} (54.6 μm and 72.5 μm) associated with translational modes. We also detected another weak absorption near 273 cm^{-1} (36.6 μm). Absorption coefficients for solid crystalline NH_3 in the far-IR have been published (Sill et al. 1980) and optical constants have been summarized by Martonchik et al. (1984).

CO_2 films condensed at 13 K produced an amorphous ice with a single absorption band at 117 cm^{-1} (85.5 μm). The ice transformed irreversibly to a crystalline phase between 60 K and 65 K. Our data are in good agreement with the results of Kuan (1969) who discussed changes in the far-IR spectrum of solid CO_2 at temperatures below 77 K. The 117 cm^{-1} band is associated with a translational lattice mode (e.g. see Brown & King 1970). Other data on CO_2 in the 77 K region have been reported by Anderson & Gebbie (1965) and Ron & Schnepp (1967). The optical constants of CO_2 ice in the far-IR, with an emphasis on values for temperatures above 77 K, are summarized by Warren (1986).

Amorphous H_2CO ice condensed at 13 K has a single broad absorption at 164 cm^{-1} (61 μm). Amorphous deposits evolved into a multi-peaked spectrum of crystalline H_2CO when the temperature was increased to the 75 K region with peaks at 219, 179, and 163 cm^{-1} (45.7, 55.9, and 61.3 μm). When recooled to T = 13 K, the peaks were generally sharper and blue shifts of up to 5 cm^{-1} were observed resulting in the 13 K detection of the 103 cm^{-1} band attributed to a translational lattice mode (Weng et al. 1989). Our results for crystalline H_2CO at both 77 K and at 13 K are in good agreement with recently reported peak positions in the far-IR by Weng et al. (1989).

4.2. *Ice mixtures*

Our results show that the far-IR spectra of pure CH_3OH, NH_3, CO_2, and H_2CO in the amorphous and crystalline phases are unique, but the distinctive spectral characteristics of these molecules are suppressed in mixed ices in 12:100 ratios with H_2O. Although spectra of mixtures might be expected to reflect the sum of their weighted

components, in fact we have shown there is little variation from the amorphous spectrum of pure H_2O even when a second component made up 50% of the mixture.

When the ice mixtures are annealed to form a crystalline phase, the resulting spectra are nearly identical to the spectrum of pure crystalline H_2O which has a dominant band at 223 cm^{-1} (44.8 μm). Annealing these mixtures to 155 K would be expected to result in the loss of some fraction of the more volatile species, however, we know from laboratory experiments performed by one of us (Hudson & Donn 1991) that varying amounts of trapped gases can still be retained by H_2O ice. The FWHM of the mixtures are within 20% of the FWHM of pure H_2O ice. Another parameter we measured was the absorbance ratio of the principal maximum to the well resolved secondary maximum (162 cm^{-1}, 61.7 μm) in crystalline pure H_2O ice. The same ratio in the mixtures is always smaller. The $H_2O + CO_2$ and $H_2O + CO$ ices did not develop the secondary maximum, only a weak shoulder in the 162 cm^{-1} area. Since spectra have not been corrected for reflection losses, absolute values for the FWHM and the ratio values for each ice mixture are not meaningful.

The most unique far-IR result came from the study of $H_2O + CH_3OH$ (100:50) mixtures. Amorphous deposits of this ice evolved during slow warming into a multi-peaked spectrum we have associated with the methanol clathrate hydrate (Hudson & Moore 1993), based on an earlier identification by Blake et al. (1991). Our spectra of multi-component ices show that the clathrate hydrate peaks are weakened in the presence of additional molecular species which probably interfere with the formation of the clathrate structure during warming.

Results from our proton irradiation experiments demonstrates that the far-IR multi-line spectrum associated with the CH_3OH clathrate hydrate structure becomes less intense as the radiation dose is increased. These results are reminiscent of the amorphization of crystalline water ice due to ion irradiation (Moore & Hudson 1992; Baratta et al. 1991 and Strazzulla et al. 1992). Our results also show that the clathrate structure does not reform when the irradiated ice is warmed possibly due to the fact that the ice is "contaminated" with radiation products which interfere with the reformation of the clathrate structure. This interpretation was supported by additional experiments in which a freshly-condensed amorphous ice (composed of $H_2O + CH_3OH$, 100:50) was irradiated after which it failed to form the clathrate structure during warming.

5. Conclusion

We present a large number of far-IR spectra of ices made and studied with a single experimental procedure which used a self-consistent set of deposition, warming rates, and annealing temperatures. Our results include spectra of astrophysically relevant pure and mixed ices in both the amorphous and crystalline phases. It is believed that this set of data will help connect the current fragmentary state of the literature of far-IR laboratory measurements.

Our results show that in the far-IR region we studied, the spectral features of each pure ice is unique in both the amorphous and crystalline phases. The far-IR data includes peak positions of pure ices which can be matched with far-IR observations to search for likely candidates. The plot of the reversible changes in the peak frequency with temperature for several crystalline ice absorptions shows that these peak positions are directly related to the temperature of the ice.

In H_2O-dominated icy mixtures with 12% of an added molecule, the amorphous and crystalline spectra are nearly identical with the spectrum of pure H_2O ice. We conclude that the observation of a single broad absorption centered near 222 cm^{-1} in an extra-terrestrial source cannot be uniquely fitted with the spectrum of either pure H_2O or of an H_2O-dominated mixture, since the difference between the peak positions of these ices is only a few cm^{-1}. Also amorphous-like H_2O ice spectra could result from low temperature deposits or from radiation amorphization of crystalline ices, therefore conclusions on the thermal history of ices are not possible. The dramatic sharpening observed in the principal maximum during crystallization in both pure H_2O and H_2O-dominated ices can be used to identify the crystalline phase. Again, however, discriminating between pure H_2O and H_2O-dominated mixtures is quite difficult. The idea that two peaks are required for crystalline H_2O-dominated ice mixtures was the rule for most of our simple binary ices, but both $H_2O + CO_2$ and $H_2O + CO$ ice mixtures were the exception to the rule. The weakness or total absence of the secondary maximum may be one of the few discernible clues to icy mixture identifications in the far-IR especially those containing CO_2 and /or CO. Further laboratory studies are required to determine what role the concentration of impurities plays in the strength of the secondary maximum after crystallization.

Unique to this study are spectra which show the results on the effects of impurities and proton irradiation on the intensity of the unusual multi-line spectrum of an $H_2O + CH_3OH$ (100:50) ice we associated with the methanol clathrate hydrate. We observed decreases in the intensity of this multi-line spectrum due to the presence of impurities within the condensed ice mixture and decreases in the intensity of the multi-line spectrum with increased irradiation (with laboratory doses of 10^{13} to 10^{15} protons cm^{-2})*. These results suggest that the detection of this multi-line spectrum in an interstellar region

* These laboratory doses are equivalent to $\sim 10^4$ to 10^6 years of cosmic-ray exposure for interstellar materials. This is calculated from an estimate (e.g. Strazzulla et al. 1983) that near 1 MeV cosmic-ray protons have a flux of 10 cm^{-2} s^{-1}

would mean the icy mixtures have experienced little radiation amorphization and that there is a relatively low concentration of impurities (<10%) compared to H_2O and CH_3OH. A search for the multi-line features in the far-IR is encouraged. Protostars NGC 7538 IRS 9, and W33A (Allamandola et al. 1992) may be good candidates since they contain a significant amount of CH_3OH. Allamandola et al. (1992) point out that after H_2O, CH_3OH is the most abundant condensate in these observed sources even though the actual ratio of H_2O to CH_3OH varies between protostars and depends on which mid-IR bands are ratioed.

The use of the ESA/ISO space based telescope is on the horizon; it should be launched in 1995. It will observe within the 500 cm^{-1} (20 μm) to 100 cm^{-1} (100 μm) region. The huge reduction in background flux expected for ISO in orbit and the anticipated improved sensitivity due to stable pointing and lack of atmospheric blur should result in extremely high quality far-IR observations. It remains our best opportunity for an examination of far-IR sources in search of interstellar ices.

Acknowledgements. We thank Bert Donn for numerous discussions and a critical reading of the manuscript. We recognize the help of Bill Glacuum from whom we obtained many references to the far-IR literature. We acknowledge the receipt of a thesis containing relevant far-IR data from Mayo Greenberg. The authors thank Steve Brown and members of the GSFC/Radiation Facility for operation of the accelerator. R.L.H. acknowledges the Administration of Eckerd College for a leave during which this work was done under an intergovernmental Personnel Act Agreement at the NASA/Goddard Space Flight Center. We acknowledge NASA funding support through Grant NSG 5172.

References

Allamandola L.J., Sandford S.A., Tielens A.G.G.M., Herbst T.M. 1992, ApJ 339, 134
Anderson A., Gebbie H.A. 1965, Spectrochimica Acta 21, 883
Anderson A., Andrews B., Meiering E.M., Torrie B.H. 1988, J. Raman Spectrosc. 19, 85
Anderson A., Walmsley S.H. 1965, Mol. Phys. 9, 1
Baratta G.A., Leto G., Spinella F., Strazzulla G. and Foti G. 1991, A&A 252, 421
Bertie J.E., Labbe H.J., Whalley E. 1969, J. Phys. Chem. 50, 4501
Binbrek O.S., Anderson A. 1972, Chem. Phys. Let. 15, 421
Blake D., Allamandola L., Sandford S., Hudgins D., Freund F. 1991, Sci. 254, 548
Breukers R. 1991, Thesis Univ. of Leiden, Leiden, The Netherlands
Brown K.G., King W.T. 1970, J. Chem. Phys. 52, 4437
Cruikshank D.P. et al. 1991, BAAS 23, 1208
Dempster A.B., Zerbi G. 1971, J. Chem. Phys. 54, 3600
d'Hendecourt L.B., de Muizon M.J. 1989, A&A 223, L5
Drapatz S., Haser L., Hofmann R., Oda N., Iyengar K.V.K. 1983, A&A 128, 207
Durig J.R., Pate C.B., Li Y.S., Antion J. 1971, J. Chem. Phys. 54, 4863
Erickson E.F., Knacke R.F., Tokunaga A.T., Hass M.R. 1981, A&A 245, 148
Ferraro J.R., Sill G., Fink U. 1980, Applied Spect. 34, 525
Forveille T., Morris M., Omont A. and Likkel L. 1989, A&A 176, L13
Geballe T.R., Kim Y.H., Knacke R.F. and Noll K.S. 1988, ApJ 326, L65
Graham J.A., Chen W.P. 1991, AJ 102, 1405
Hodapp K.W., Sellgren K. and Nagata T. 1988, ApJ 326, L61
Hudgins D.M., Sandford S.A., Allamandola L.J. 1993, ApJ Suppl. Ser. 86, 713
Hudson R.L., Donn B. 1991, Icarus 94, 326
Hudson R.L., Moore M.H. 1992, J. Phys. Chem. 96, 6500
Hudson R.L., Moore M.H. 1993, ApJ 404, L29
Kitta K., Krätschmer W. 1983, A&A 122, 105
Kuan T.S. 1969, PhD Thesis, Univ. Southern Calif.
Martonchik J.V., Orton G.S., Appleby J.F. 1984, Applied Optics 23, 541
Moore M.H., Hudson R.L. 1992, ApJ 401, 353
Omont A., Moseley S.H., Forveille et al. 1990, ApJ 355, L27
Owen T. et al. 1992, BAAS 24, 961
Papoular R., Lena P., Marten A., Rouan D., Wijnbergen J. 1978, Nature 176, 593
Redding F.P., Hornig D.F. 1951, J. Chem. Phys. 19, 594
Ron A., Schnepp O. 1967, J. Chem. Phys. 47, 3991
Rouan D., Omont A., Lacombe F. and Forveille T. 1988, A&A 189, L3
Savoie R., Fournier R.P. 1970, Chem. Phys. Lett. 7, 1
Sill G., Fink U., Ferraro J.R. 1980, J. Opt. Soc. Am. 70, 724
Strazzulla G., Calcagno L., Foti G. 1983, MNRAS 204, 59P
Strazzulla G., Baratta G.A., Leto G., Foti G. 1992, Europhys. Let 18, 517
Tielens A.G.G.M. 1989, in Interstellar Dust, ed. L.L. Allamandola, A.G.G.M. Tielens, Proc. IAU Symp. 135, Kluwer Academic Press, Dordrecht, p. 239
Warren S.G. 1986, Appl. Opt. 25, 2650
Weng S.X., Anderson A., Torrie B.H. 1989, J. Raman Spect. 20, 789
Wong P.T.T., Whalley E. 1971, J. Chem. Phys. 55, 1830

Table 1. The positions of absorption peaks observed in the 500 cm^{-1} (20 μm) to 100 cm^{-1} (100 μm) region for several molecular ices in both the amorphous (Fig. 2) and crystalline (Fig. 3) phases

MOLECULAR ICE	TEMPERATURE (K)	PHASE	PEAK WAVENUMBER (cm^{-1})
H_2O	13	AMORPHOUS	220
	13/155/13	CRYSTALLINE	230, 162
CH_3OH	13	AMORPHOUS	321, 148
	14/130/14	CRYSTALLINE	353, 175, 147, 113
NH_3	14	AMORPHOUS	423
	14/70/14	TRANSITION	422,372
	77/13	CRYSTALLINE	352
CO_2	13	AMORPHOUS	117
	13/65/13/	CRYSTALLINE	117
H_2CO	13	AMORPHOUS	164
	13/85/13	CRYSTALLINE	223, 191 sh, 180, 164, 103

Table 2. The positions of absorption peaks observed in the 500 cm^{-1} (20 μm) to 100 cm^{-1} (100 μm) region for H_2O-dominated molecular ice mixtures in both the amorphous and crystalline (Fig. 5) phases; peak frequencies for pure H_2O are included for comparison

MOLECULAR ICE		PHASE	PEAK WAVENUMBER (cm^{-1}), T=13 K
H_2O	(PURE)	AMORPHOUS	220
		CRYSTALLINE	230,162
$H_2O + CH_3OH$	(100:12)	AMORPHOUS	211
		CRYSTALLINE	230, 170
$H_2O + NH_3$	(100:12)	AMORPHOUS	218
		CRYSTALLINE	412, 343, 230, 170
$H_2O + CO_2$	(100:12)	AMORPHOUS	219
		CRYSTALLINE	231, 194 sh, 168 sh
$H_2O + H_2CO$	(100:12)	AMORPHOUS	216
		CRYSTALLINE	230, 195 sh, 164
$H_2O + CH_4$	(100:12)	AMORPHOUS	218
		CRYSTALLINE	231, 164
$H_2O + CO$	(100:12)	AMORPHOUS	215
		CRYSTALLINE	232

Table 3. The positions of absorption peaks observed in the 500 cm^{-1} (20 μm) to 100 cm^{-1} (100 μm) region for the CH_3OH clathrate hydrate ice at different temperatures, in the presence of additional molecules, and after irradiation; these peak frequencies correspond to spectra in Figs. 8, 9 and 10

MOLECULAR ICE	TEMP. (K)	FIG. #	PEAK WAVENUMBER (cm^{-1})
CH_3OH clathrate hydrate	13	8f,10a	327, 275, 232*, 214 176, 153, 129
CH_3OH clathrate hydrate	148	9a	312, 267, 223*, 213, 168, 124
H_2O+CH_3OH+CO+NH_3 (100:50:2:2)	155	9b	313, 264, 220*, 211, 172, 124
H_2O+CH_3OH+CO+NH_3 (100:50:~9:2)	150	9c	313, 267sh, 220*, 213
CH_3OH clathrate hydrate after 1x10^{13} p^+ cm^{-2}	13	10b	324, 275, 231*, 214, 177, 153, 130
CH_3OH clathrate hydrate after 1x10^{14} p^+ cm^{-2}	13	10c	317sh, 265sh, 219
CH_3OH clathrate hydrate after 1x10^{15} p^+ cm^{-2}	13	10d	206
IRRADIATED CH_3OH clathrate hydrate, REWARMED	133	10e	216
IRRADIATED CH_3OH clathrate hydrate, ANNEALED	13	10f	232, 176

* peak position corresponds to crystalline H_2O ice